2024 IEEE/RSJ International Conference on Intelligent Robots and Systems (IROS)
October 14-18, 2024. Abu Dhabi, UAE

An Active and Dexterous Bionic Torso for a Quadruped Robot *

Ruyue Li, Yaguang Zhu, *Member, IEEE*, Yuntong Wang, Zhimin He and Mengnan Zhou

***Abstract*—The torso of quadruped mammals serves as a robust foundation for their bodies, enabling a diverse array of agile and intricate movements. However, current quadruped robots cannot match the extensive range of motion exhibited by biological torsos while also serving a load-bearing role. Therefore, this paper presents an active bionic torso that emulates the quadrupedal animal's spinal column and associated muscular structure. This innovative torso can mimic animal torsos movements, including flexing, extending, lateral bending, and axial rotation. A thorough analysis of the torso's kinetic, workspace, and structural dynamics has been conducted. This proposed torso boasts a considerable load-bearing capacity and can support a load that exceeds its weight tenfold. The passive spring incorporated into the bionic torso emulates the intervertebral discs' shock-absorbing and load-bearing functions. Additionally, this paper documents the development of a quadrupedal robot fitted with the proposed bionic torso, demonstrating the torso's mobility in a real-world application.**

I. Introduction

The high-dynamic motion of quadruped animals in the natural world is inseparable from agile torsos. Anatomical studies [1] reveal that the torso comprises the spine, functional bones, visceral organs, and muscles. The coordinated action of the spine and muscles provides support for the animal's body, aiding in maintaining specific postures and enabling a variety of complex movements. With the deepening research on the physiological structure and locomotion principles of quadruped animals, an increasing number of spine-inspired quadruped robots based on biomimetic principles have been developed [2]-[6]. Numerous studies suggest that the flexible movement of the spine contributes to enhancing the dynamic performance [7], postural stability [8], and energy utilization efficiency [9] [10] [11] of quadruped robots.

However, when designing biomimetic spine-type quadruped robots, most researchers focus solely on imitating the structural morphology or movement functions of the lumbar vertebrae within the spine. This limitation results in existing biomimetic spines, whether featuring a flexible multi-joint structure mimicking vertebrae [4][5][6] or an articulated single-joint structure [2][3], having relatively limited degrees of freedom. These biomimetic spines can either mimic the flexion-extension movement of the biological spine [3][4][5] or only achieve the lateral bending observed in the biological spine [12] [13]. In reality, the biological spine exhibits lateral bending and flexion-extension functions in the lumbar vertebrae as well as axial rotational activity [14] [15] in cervical. The current joint-type spines cannot replicate the bending, extension, lateral bending, twisting, and various compound movements of the biological torso. Furthermore, existing biomimetic spine designs focus solely on realizing spine movement functions, neglecting the spine's role in supporting the body and bearing external pressures. This oversight may lead to the robot's inability to maintain body stability during dynamic motion or external force impact.

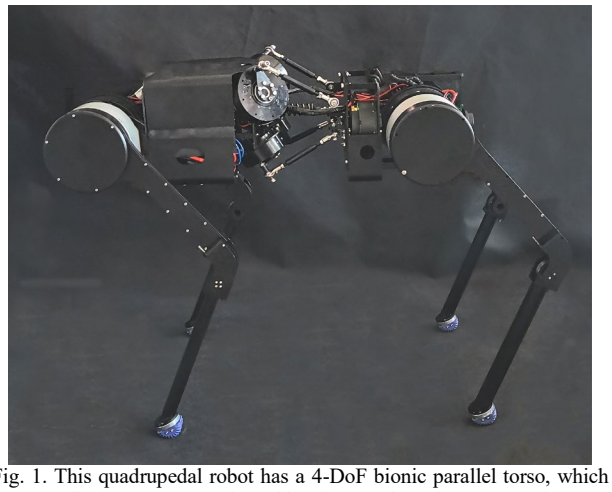

Fig. 1. This quadrupedal robot has a 4-DoF bionic parallel torso, which supports flexion, extension, lateral bending, and axial torsion motions.

To bridge this gap, we designed an active and dexterous bionic torso. This torso is developed based on the principles of animal torso movement and physiological structures. The animal torsos maintain posture and execute movements through the coordinated actions of the spine and muscles. The spine provides support for the body and enables various movements. The skeletal structure moves when muscles contract and relax. The bionic torso we designed features a spring-loaded pillar mimicking the vertebral column and active chains emulating muscle groups. In addition, the torso can mimic the movements of biological torsos. We have also developed a quadruped robot equipped with an active biomimetic torso. (See Fig.1.). The main contributions of this paper include:

- A novel bionic active torso is designed to mimic the animals' torsos, which include a spine and muscles. The pillars with springs imitating the spine bear the load, and the motors are used like muscles to generate active movements.
- The proposed torso can perform bionic motion, including flexing, extending, lateral bending, and axial rotation. Its ranges of motion for lateral bending and flexion-extension are significantly greater than those of cats and horses. This torso can withstand axial loads ten times its weight.

* This work is supported by the National Natural Science Foundation of China under Grant 62373064, in part by the Fundamental Research Funds for the Central Universities under Grant 300102259308 and 300102259401.The authors are with the Key Laboratory of Road Construction Technology and Equipment of MOE, Chang'an University, Xi'an 710064, China (e-mail: liruyue, zhuyaguang, wangyuntong, hezhimin, zhoumengnan@chd.edu.cn).
Corresponding author: Y. Zhu (zhuayaguang@chd.edu.cn)

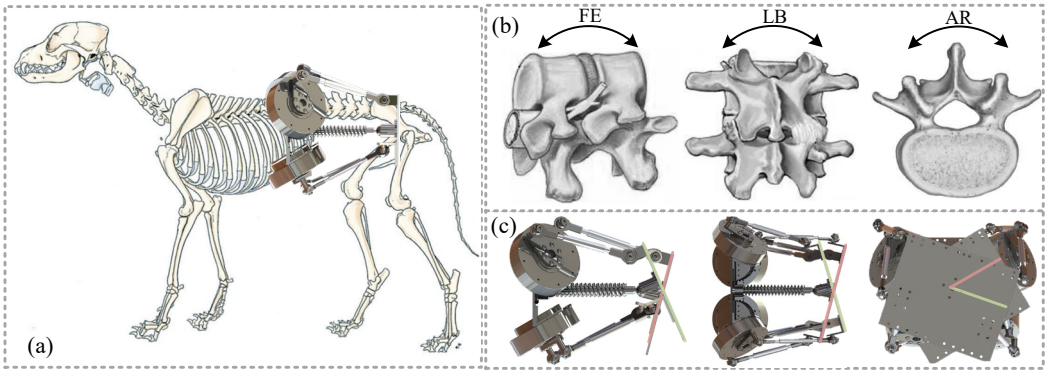

Fig. 2. (a) Torso Bionic Schematic [1], (b) forms of movement of the animal's torso [15], AR is for Axial Rotation, FE is for Flexion/extension, LB is for Lateral Bending, (c) bionic motion of the proposed torso, include pitching, yawing, twisting.

- The kinematics, motion space, dexterity, and amplitude-frequency characteristics of the proposed active torso are analyzed. A quadruped robot configured with an active torso is developed and validated.

The remaining sections of this paper are organized as follows: Section II introduces the bionic design and kinematics of the active torso. Section III analyzes and compares the characteristics of the torso. Section IV establishes the force-position control architecture of the proposed torso. Section V experimentally verifies the bionic function of the torso and its applicability to quadrupedal robots. Finally, Section VI concludes this paper.

II. Design of Bionic Torso

The torso of quadruped mammals engaged in high-speed running not only bears its weight but also achieves a wide range of movements. To address the limitations in motion capabilities imposed by the rigidity or single degree of freedom in most quadruped robot torsos, we propose an actively dexterous parallel mechanism of the 4RSS-1PS type (R - revolute joint, S - spherical joint, P - prismatic joint) as a bionic torso (Fig. 2. (a)) of a quadruped robot. This torso can perform various bionic movements.

A. Bionic Torso

The configuration and functionality of the proposed bionic torso are designed based on the anatomical principles of biological torsos. The bionic torso consists of a moving platform, a static platform, four active chains, and a retractable pillar with springs. The two platforms are parallel to each other and connected by four active chains and the pillar. Anatomical studies [1] [15] of canids reveal that the spinal muscles, dorsal and ventral muscles surrounding the torso work in coordination to maintain torso stability and articulate the skeletal structures within the torso for bending, extending, rotation, and lateral bending movements (Fig. 2. (b)). The four branches designed in the bionic torso imitate the distribution of muscle groups on the animal's torso. The coordinated motion of the four branched chains with active drive allows the bionic torso to perform actions such as pitching, yawing, and twisting (Fig. 2. (c)), corresponding to all the functional movements of the animal's torso. The central pillar of the torso mimics the animal's spine, providing primary support for the body [16] and allowing the torso to flex and rotate through a ball-and-hinge joint. The spring attached to the pillar simulates the cushioning and stabilizing functions of the intervertebral discs [17] within the animals' spine. Furthermore, the bionic torso can also achieve axial movement due to the physiological mechanism where the distances between vertebrae change as the animal moves [18]. Thus, this torso has 4 Degree of Freedom (DoF). The multiple postural movements of the torso contribute to the dynamic balance and stability of robotic maneuvers, facilitate rapid turning to adapt to environmental changes, and optimize load distribution for enhanced energy efficiency.

The bionic torso proposed in this paper is optimized and designed based on the 6-DoF parallel torso (Fig. 3. (a)) we previously developed [19] [25]. In contrast, the 4-DoF torso is more lightweight and compact, with its structural functionality resembling that of a biological torso more closely. Although it experiences a slight decrease in stability compared to the 6-DoF torso, there is a substantial enhancement in its mobility. The physical model and geometric configuration of the

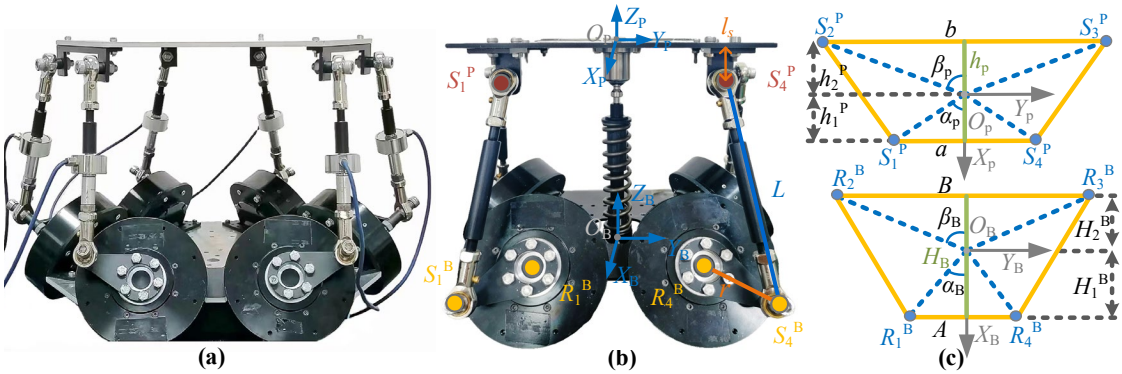

Fig. 3. Torso model. (a) 3D model of 6-DoF parallel torso, (b) 3D model of 4-DoF parallel torso, (c) geometric configuration of static platform and moving platform.

proposed torso are depicted in Fig. 3. (b) and (c). It has a mass of 3.1 kilograms and a volume of 27 cm × 23 cm × 21 cm. Each limb of the torso is structurally identical, consisting of a rocker, two spherical hinges and a connecting rod. Position and orientation of moving platform are achieved by the coordinated movement of the connecting rods, which is driven by the rotation of the rockers. The motors are arranged in a trapezoidal configuration fixed on the static platform, with the motor axes inclined at an angle of 30° (γ) relative to the static platform surface. The center points R_i^B of the output joints of the four motors, projected onto the static platform, form a trapezoid with a top base A, a bottom base B, and a height H_B. The center points S_i^P of the spherical hinges at the top of the four connecting rods, when projected onto the dynamic platform, configure a trapezoid with a top base a, a bottom base b, and a height h_p. The central pillar of the torso is fixed at the centroid of the static platform at the lower end and connected to the centroid of the moving platform at the upper end through a universal ball joint. The spring attached to the pillar has a stiffness coefficient K of 15 N/mm. To facilitate the description of the kinematics of the torso, Cartesian coordinate systems $\{B\}$ and $\{P\}$ with origin points O_B and O_P, respectively, are established at the centroids of the static and moving platforms. The coordinate systems $\{B\}$ and $\{P\}$ are parallel in space. The Z_B axis is directed along the line connecting the centroids of the moving and static platforms, pointing towards the moving platform. The Z_P axis aligns with the direction of Z_B. The directions of the X-axes and Y-axes are as indicated in Fig. 3. (c). S_i^P represents the center of the upper spherical hinge, S_i^B represents the center of the lower spherical hinge, and R_i^B represents the center of the rotational joint at the motor output end.

B. Inverse Kinematics

The inverse kinematics [19] of the proposed torso can be expressed as $\boldsymbol{\theta}_i = f_1(Z, \varphi, \theta, \psi)$, i=1, 2, 3, 4. The detailed procedure for solving the joint angle θ_i for each chain is elaborated as follows with the known body postures (Z, φ, θ, ψ). Each intermediate parameter of the moving platform is calculated as follows. α_B=arctan (A / 2 H_1^B), β_B= arctan (B / 2 H_2^B), α_P=arctan (a / 2 h_1^P), β_P= arctan (b / 2 h_2^P), where A= 0.11m, B=0.211m, a=0.135m, b=0.198m, H_1^B =0.079m, H_2^B =0.041m, h_1^P =0.049m, h_2^P =0.08m.

$$l_i^B = \begin{cases} \sqrt{\left(\frac{A}{2}\right)^2 + \left(H_1^B\right)^2}, i = 1,4 \\ \sqrt{\left(\frac{B}{2}\right)^2 + \left(H_2^B\right)^2}, i = 2,3 \end{cases} \tag{1}$$

$$l_i^p = \begin{cases} \sqrt{\left(\frac{a}{2}\right)^2 + \left(h_1^p\right)^2}, i = 1,4 \\ \sqrt{\left(\frac{b}{2}\right)^2 + \left(h_2^p\right)^2}, i = 2,3 \end{cases} \tag{2}$$

The description of point R_i^B in the coordinate system $\{B\}$ and the description of point S_i^P in the coordinate system $\{P\}$ can be written as

$$\begin{cases} O^B R_i^B = \left[l_i^B \cos\omega_i, l_i^B \sin\omega_i, l_r \right] \\ O^P S_i^p = \left[l_i^p \cos\sigma_i, l_i^p \sin\sigma_i, -l_s \right] \end{cases} \tag{3}$$

where ω_i = {-α_B, -(π-β_B), -(π+β_B), α_B}, σ_i = {-α_P, -(π-β_P), -(π+β_P), α_P}, l_s=0.022m, l_r=0.023m. l_r denotes the height of point R_i^B from the static platform and l_s denotes the distance of point S_i^B from the plane of the moving platform. If the position and orientation [X, Y, Z, φ, θ, ψ] of the moving platform in the coordinate system $\{B\}$ is known, then the vectors $O^B S_i^P$ as well as the rotation matrix ${}_P^B T$ between the coordinate system $\{P\}$ and $\{B\}$ are known.

$$O^B S_i^p = {}_p^B T \cdot O^p S_i^p + C \tag{4}$$

$${}_p^B T = \begin{bmatrix} c\varphi c\theta c\psi - s\varphi s\psi & -c\varphi c\theta s\psi - s\varphi c\psi & c\varphi s\theta \\ s\varphi c\theta c\psi + c\varphi s\psi & -s\varphi c\theta s\psi + c\varphi c\psi & s\theta s\varphi \\ -s\theta c\psi & s\theta s\psi & c\theta \end{bmatrix} \tag{5}$$

where C is the position vector of O^P in the coordinate system $\{B\}$. *sin* and *cos* are abbreviated as s and c, respectively. The direction vector of the motor output axis in the coordinate system $\{B\}$ is

$$U_i = \left[\frac{l_r}{\tan\gamma}\cos\zeta, \frac{l_r}{\tan\gamma}\sin\zeta, l_r \right], \left(i = 1,2,3,4\right) \tag{6}$$

where ζ = {0, -2π/3, -4π/3, 0} corresponds to the orientation angles for each motor. Establishing a new reference frame at the center of rotation for the motor joints, the direction vectors for each coordinate axis are represented as follows

$$X_i^B = \begin{cases} \frac{U_i \times Z^B}{|U_i \| Z^B|}, i = 1,3 \\ \frac{Z^B \times U_i}{|U_i \| Z^B|}, i = 2,4 \end{cases}, Y_i^B = \frac{U_i \times X_i^B}{|U_i \| X_i^B|}, Z^B = [0,0,1] \tag{7}$$

The position vector of the rocker $R^B S_i^B$ relative to $\{B\}$ is given by $R^B S_i^B = r(X_i^B \cos\theta_i + Y_i^B \sin\theta_i)$, where r refers to the rocker length and is 0.041m. Based on $O^B S_i^P$ and $O^B R_i^B$, $R^B S_i^P$ and $S^B S_i^P$ can be represented as follow.

$$R^B S_i^p = O^B S_i^P - O^B R_i^B \tag{8}$$

$$S^B S_i^P = R^B S_i^P - R^B S_i^B \tag{9}$$

According to the cosine theorem, $S_i^B S_i^P$ can be expressed by the following equation

$$\left|S_i^B S_i^P\right|^2 = L^2 = r^2 - 2R_i^B S_i^P \cdot R_i^B S_i^B + \left|R_i^B S_i^P\right|^2 \tag{10}$$

Define $\Lambda_i = L^2 - r^2 - \left|R_i^B S_i^p\right|^2$, The above equation can be expressed as

$$\Lambda_i + 2R_i^B S_i^p \cdot r(X_i^B \cos\theta_i + Y_i^B \sin\theta_i) = 0 \quad (11)$$

If $\chi = \tan(\theta_i/2)$, it can be rewritten as

$$\begin{aligned} &\chi^2\left(\Lambda_i - 2rX_i^B \cdot R_i^B S_i^p\right) + \chi(4rY_i^B \cdot R_i^B S_i^p) \\ &+2r_i^B \cdot R_i^B S_i^p + \Lambda_i = 0 \end{aligned} \quad (12)$$

Thus, the equation can be solved, and θ_i is equal to 2arctanχ.

C. Forward Kinematics

The forward kinematics for the torso calculates the moving platform's position and orientation using the Newton-Raphson [19] technique, based on the specified joint angles. To distinguish from the inverse kinematics solution process, here $\hat{\cdot}$ is used to represent the variables. When the joint angles of the four branched chains are known, the following variables can be directly obtained.

$$\begin{cases} \hat{R}_i^B \hat{S}_i^B = \hat{r}(\hat{X}_i^B \cos\hat{\theta}_i + \hat{Y}_i^B \sin\hat{\theta}_i) \\ \hat{O}^B \hat{S}_i^B = \hat{O}^B \hat{R}_i^B + \hat{R}_i^B \hat{S}_i^B \\ \hat{S}_i^B \hat{S}_i^P = \hat{O}^B \hat{S}_i^P - \hat{O}^B \hat{S}_i^B \end{cases} \quad (13)$$

Based on the principle of equal rod lengths, the equation $L^2 = \left|\hat{O}^B \hat{S}_i^P - \hat{O}^B \hat{S}_i^B\right|^2$ can be established, and after transformation, this equation becomes

$$\begin{aligned} &|{}_P^B\hat{T} \times \hat{O}^P \hat{S}_i^P + \hat{C} - \hat{O}^B \hat{R}_i^B - r\cos\hat{\theta}_i \hat{X}_i^B - r\sin\hat{\theta}_i \hat{Y}_i^B|^2 \\ &-|L_2|^2 = 0 \end{aligned} \quad (14)$$

By simultaneously solving the equations of the four chains through iteration, the position and orientation information of the moving platform $[\hat{Z}, \hat{\varphi}, \hat{\theta}, \hat{\psi}]$ can be obtained. The forward kinematics of the bionic torso can be abbreviated as $[\hat{Z}, \hat{\varphi}, \hat{\theta}, \hat{\psi}] = f_2(\theta_i), i = 1,...,4$.

D. Jacobi Matrix

The velocities of joints in joint space and the moving platform in task space are $\dot{\boldsymbol{\theta}} = \begin{bmatrix} \dot{\theta}_1 & \dot{\theta}_2 & \dot{\theta}_3 & \dot{\theta}_4 \end{bmatrix}^{\mathrm{T}}$ and $\mathbf{v} = \begin{bmatrix} \dot{z}_P & \dot{\alpha} & \dot{\beta} & \dot{\gamma} \end{bmatrix}^{\mathrm{T}}$. The mapping relationship between the joint space and the task space is given by $\mathbf{v} = \mathbf{J}(\theta)\dot{\boldsymbol{\theta}}$, where $\mathbf{J}$ is a 4×4 Jacobian matrix, a linear mapping between $\mathbf{v}$ and $\dot{\boldsymbol{\theta}}$. Thus, Jacobian matrix $\mathbf{J}$ can be obtained by

$$\mathbf{J}(\theta) = \frac{\mathbf{v}}{\dot{\boldsymbol{\theta}}} = \begin{bmatrix} \frac{\partial z_P}{\partial \theta_i} & \frac{\partial \alpha}{\partial \theta_i} & \frac{\partial \beta}{\partial \theta_i} & \frac{\partial \gamma}{\partial \theta_i} \end{bmatrix} \quad (15)$$

III. BIONIC TORSO CHARACTERIZATION AND COMPARISON

A. Movement Space

Given that the active bionic torso possesses 4-DoF, we separately utilize positional and postural spaces to delineate the workspace of the torso. The range of motion along the Z-axis is independent of orientation variations. For computational ease, all orientation angles are set to 0°, the range of Z motion is [0.139m, 0.209m]. With the torso platform positioned at X=0m, Y=0m, Z=0.1579m, the orientation range is $\varphi \in$[-39°, 39°], $\theta \in$[-60°, 60°], $\psi \in$[-41°, 41°] (see Fig. 4. (a)). Compared to the previous 6-DoF torso orientation space ($\varphi \in$[-34°, 34°], $\theta \in$[-18°, 14°], $\psi \in$[-16°, 16°]) (see Fig. 4. (b)), the flexion-extension and axial rotation ranges of the 4-DoF torso are approximately 2.5 times larger. However, the lateral bending range of the two torsos is comparable. We also compare the proposed torso's posture space with that of a cat [20] and a horse [21]. The results (Fig. 4. (c)) indicate that the proposed torso exhibits superior flexion-extension and lateral bending capabilities compared to the other torsos. Although the axial rotation range of the bionic torso is relatively large, it still lags behind the axial rotation capability of a cat. Overall, the proposed torso achieves a level of orientation motion comparable to that of typical quadrupedal animal torsos.

B. Load Characterization

Load capacity is a crucial indicator for evaluating bionic torsos' performance. Biomechanical studies [16] [22] indicate that the spine of quadrupedal animals primarily withstands significant axial compressive loads. To validate the axial load-bearing capacity of the proposed torso, we conducted axial load tests on the torso in three different states: (*i*) with the moving platform stationary, (*ii*) with the platform moving along the Z-axis, and (*iii*) with the platform laterally bending around the X-axis. During the experiment, six 5kg weights were continuously applied to the center of the moving platform until a total load of 30kg was reached. For each increment of load, the corresponding current was recorded. The linear relationship after fitting the scattered points

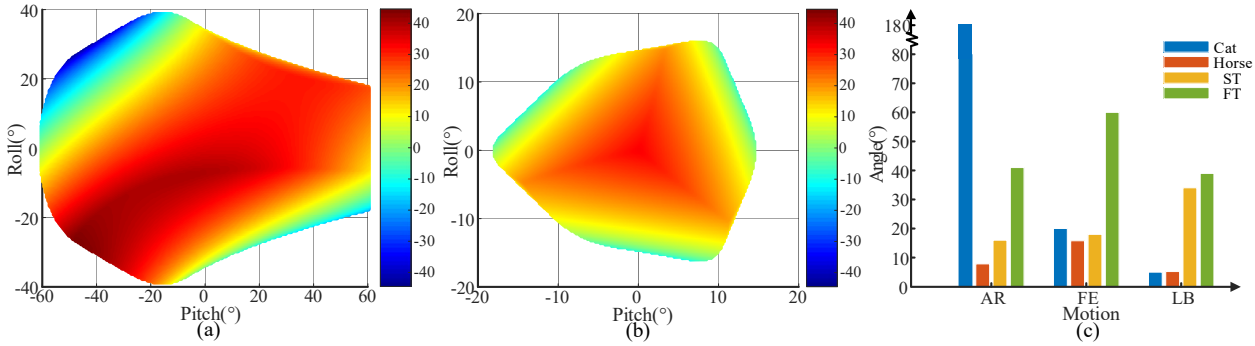

Fig. 4. Posture Movement Space. (a) for proposed 4-DoF torso, (b) for 6-DoF torso, where the color bar indicates the yaw. (c) comparison with horses and cats, AR is for Axial Rotation, FE is for Flexion/extension, LB is for Lateral Bending. ST stands for Six-DoF-Torso and FT stands for Four-DoF-Torso.

corresponding to different loads is shown in Fig. 5. Additionally, we compared the load conditions of this torso with those of the previous 6-DoF torso. It can be observed that regardless of the state of the two torsos, an increase in load leads to an increase in motor current. The motor current is generally higher when the torso undergoes lateral bending motion and is lowest during static loading. Under equivalent load conditions, the motor current of the proposed torso is more minor, indicating that the torso has a greater load capacity than the previous torso. Considering that the rated operating current of the torso's driving motor is 10.3A, it is evident that the torso can operate normally under a 300N axial load. Significantly, the torso can withstand approximately ten times its weight in axial load within its standard operating range. Certainly, the loading on the torso of quadrupeds during locomotion is diverse and intricate, extending beyond mere axial loading of the spine. In our subsequent studies, we aim to conduct an analysis of the forces acting on the torso in various other orientations.

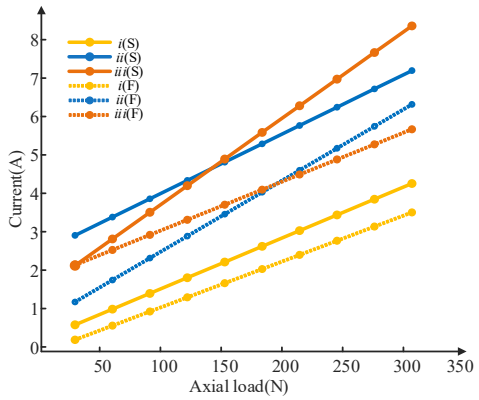

Fig. 5. Linear relationship between torso axial load and motor current. (*i*) the torso is stationary, (*ii*) the moving platform moves in the *Z*-direction, and (*iii*) the moving platform bends laterally around the *X*-direction, S stands for 6-DoF parallel torso and F for 4-DoF proposed bionic torso.

C. Dexterity

Dexterity is a critical indicator for evaluating the dynamic performance of the bionic torso. The dexterity of a torso indicates the ability of the moving platform to vary its velocity when moving in all possible directions from the current pose state. The relationship between joint space velocity and operational space velocity is expressed as follows.

$$\| \delta \mathbf{v} \| \cdot \| \mathbf{v} \|^{-1} \leqslant \| \boldsymbol{J} \| \cdot \| \mathbf{J}^{-1} \| \cdot \| \delta \boldsymbol{\theta} \| \| \boldsymbol{\theta} \|^{-1} \tag{16}$$

where $\|\boldsymbol{J}\| \cdot \|\boldsymbol{J}^{-1}\|$ represents the condition number of the Jacobian matrix, denoted as $C(\boldsymbol{J})$, $C(\boldsymbol{J}) \in (1, \infty)$. It is the amplification factor of the relative error in actuator velocity that causes the relative error in the platform velocity.

For ease of presentation, we adopt the reciprocal of the condition number of the Jacobian matrix $C(\boldsymbol{J})^{-1}$, known as the Local Dexterity Index (LDI) D_{LDI}, to describe the dexterity of the mechanism [23]. In this way, the range of D_{LDI} is constrained between 0 and 1. A value closer to 1 for the LDI indicates higher dexterity of the mechanism, implying better agility, control precision, and superior local motion performance. Fig. 6. (a) indicates that the local dexterity distribution of the proposed torso posture space is relatively dispersed, with the optimal motion dexterity concentrated in the center of the working area. In the common region of the torso's flexion-extension motion ±35° range and axial rotation ±20° range, the local dexterity values of the torso remain stable at 0.25-0.4, with a uniform and good dexterity variation. The local dexterity (Fig. 6. (b)) of the 6-DoF torso posture space exhibits uniform variation during the flexion-extension motion from -10° to 13°, with a maximum value of 0.25. Through comparison, it is evident that the proposed bionic torso pose space has a more extensive range of motion dexterity and better dexterity.

D. Amplitude-frequency Characteristics

The dynamic response of the torso system is characterized by analyzing the amplitude-frequency response of the system to various frequencies of sinusoidal input signals. The sinusoidal signal is $Z=0.158+0.013\times\sin(2\pi ft)$, and the frequency is from 0.1Hz to 22Hz. The amplitude-frequency characteristics curve of the torso system (depicted by the red line in Fig. 6. (c)) reveals that even at a frequency of 22Hz, the magnitude of the torso continues to increase. Z of the torso changes in 22Hz as Fig. 6. (d). This result indicates that the torso system responds robustly to a broader range of frequency variations. In contrast, the magnitude of the 6-DoF torso starts declining at a frequency of 16Hz, illustrating the superior amplitude-frequency characteristics of the proposed torso compared to the 6-DoF torso.

IV. Force-Position Hybrid Control

The bionic torso is actuated by position control, wherein the joint motors move according to the joint angles calculated by inverse kinematics. Considering that the spine of an animal torso must bear significant axial compression [16], we have incorporated the capacity to withstand axial loads as a design requirement for the bionic torso. Structurally, we installed a spring resembling an intervertebral disc on the retractable pillar, mimicking the spine of animals to absorb shocks and assist in load-bearing. When the moving platform is subjected to axial external force F_l moving towards the static platform, the spring is compressed, generating a spring force F_e. Beyond

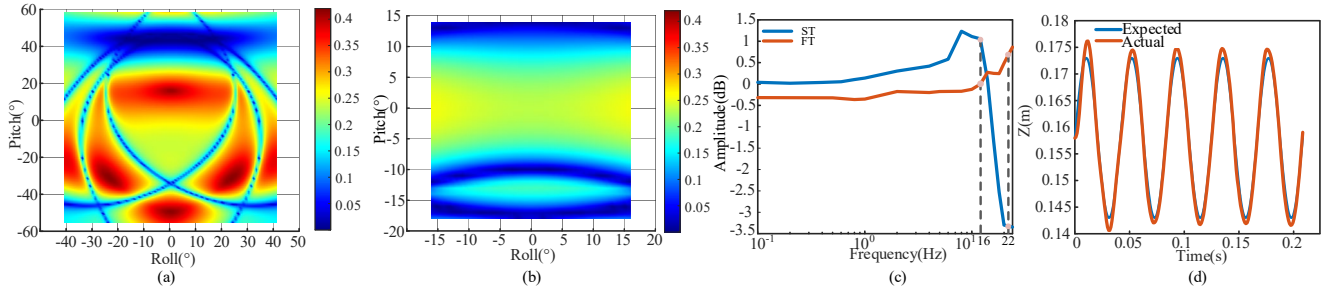

Fig. 6. Bionic torso characterization diagram. Local dexterity index (a) in proposed bionic torso posture space (*X*=0, *Y*=0, *Z*=0.185), (b) in 6-DoF torso posture space (*X*=0, Y=0, Z=0.177), (c) Bode diagram of Six-DoF-Torso (ST) and Four-DoF-Torso (FT), (d) Z of torso motion at frequency 22 Hz.

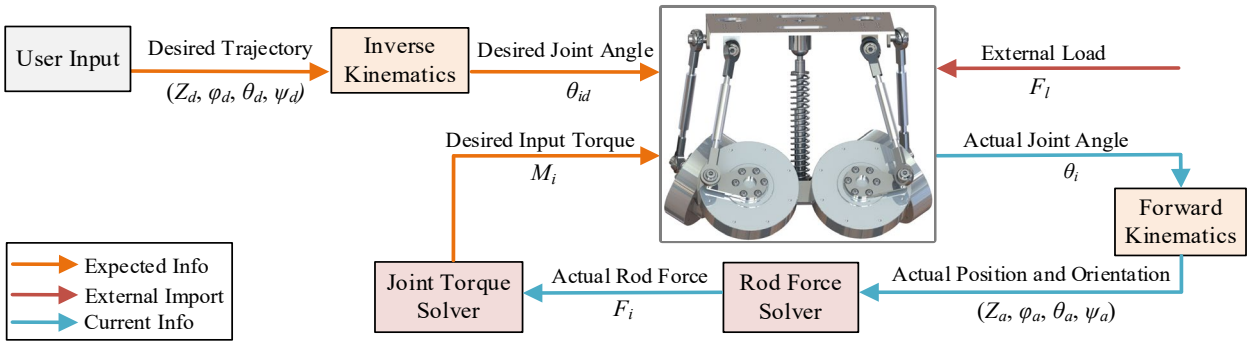

Fig. 7. The control framework for the active bionic torso.

passive load-bearing through structural design, we have also integrated a closed-loop force control mechanism based on positional control. As the torso moves while under load, the combined external forces on the moving platform and the spring force F_e collectively affect the rod force F_i, which dicate the driving torque $\boldsymbol{M}_i$ for the motor.

A. The Rod Force

The external force and moment acting on the center of mass of the moving part are defined as F_z, M_x, M_y, and M_z. F_z represents the combined force of the axial force F_l applied in the Z direction and the spring force F_e. The force F_e is calculated according to Hooke's law, where the compression of the spring is equal to the change in height of the dynamic platform. Z_0 refers to the platform's original height, and Z_a to its actual height. The force on each rod is defined as F_i, and its components are defined as F_{iz}, M_{ix}, M_{iy}, and M_{iz}. The mass of each rod is ignored. The forces applied to the center of mass of the moving part should satisfy [19]

$$\begin{cases} \sum_{i=1}^{4} F_{iz} = F_z, \quad F_z = F_l + F_e, F_e = K(Z_o - Z_a) \\ \sum_{i=1}^{4} M_{ix} = M_x, \sum_{i=1}^{4} M_{iy} = M_y, \sum_{i=1}^{4} M_{iz} = M_z \end{cases} \tag{17}$$

F_{iz}, M_{ix}, M_{iy}, and M_{iz} can be represented by F_i

$$\begin{cases} F_{iz} = (F_i \vartheta_i) \\ (M_{ix}, M_{iy}, M_{iz}) = (F_i \vartheta \times O^P S_i^P) \end{cases} \tag{18}$$

where $\vartheta_i = S^B S_i^P \cdot \left| S^B S_i^P \right|^{-1}$, it is the unit direction vector of the rod in the base coordinates. $S^B S_i^P$ can be obtained from actual joint angle θ_i and the forward kinematics. $O^P S_i^P$ is obtained by the geometric relationship. Then, the rod force F_i can be obtained by solving equations. (17) and (18).

B. Joint Torque

The desired motor torque [19] can be obtained if the force of each rod is known because the position of the motor shaft is fixed relative to the static base, as shown in Fig. 8. Plane A indicates the plane on which the input rod rotates.

Here, $\tau_i = \vartheta_i \cdot U_i$ is defined as a normal vector of the plane where the rod force and its projection lie. Then, the projection of the rod force in plane A is $n_i = U_i \cdot \tau_i$. The angle ξ_i between the force and plane A and the angle δ_i between the input rod and the force projection in plane A can be written as

$$\xi_i = \frac{\vartheta_i \cdot \boldsymbol{n}_i}{|\vartheta_i||\boldsymbol{n}_i|}, \delta_i = \frac{\boldsymbol{n}_i \cdot (-R^B S_i^B)}{|\boldsymbol{n}_i||-R^B S_i^B|} \tag{19}$$

The required torque of the motor is $\boldsymbol{M}_i = F_i r \xi_i \sqrt{1-\delta_i^2}$. The direction of the torque is determined by the coupler link force direction and the motor inclination angle.

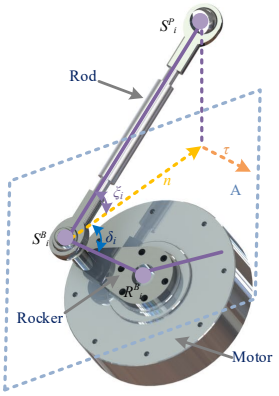

Fig. 8. Joint torque analysis of the torso.

V. EXPERIMENTAL RESULTS

We have developed a quadrupedal robot featuring a bionic torso to validate the motion of the torso. The anterior part of the robot's body comprises a storage compartment housing the power source and control board, while the posterior section hosts the bionic torso. The static platform of the torso is rigidly connected to the exoskeleton of the storage compartment, and the moving platform is fixedly attached to the frame of the robot's rear body. The robot's lower leg joints have torsion springs for shock absorption and buffering [24]. In this study, the quadrupedal robot and the bionic torso are controlled independently. We conducted load tests on the bionic torso and performed experiments on torso extension and lateral bending movements of the quadrupedal robot in a standing state.

A. Load Experiments

The bionic torso was statically positioned on the workbench for axial load testing, as shown in Fig. 9. (a). The initial pose of the torso for each motion was set as $Z = 0.158$ m, $\varphi = 0°$, $\theta = 0°$, $\psi = 0°$. A weight of mass 10 kg is placed at the center of the mass of the moving platform in place of the axial force applied. The loaded torso moves along the Z-axis in three different control modes: (*i*) position control without spring (Fig. 9. (a)), (*ii*) force-position hybrid control without

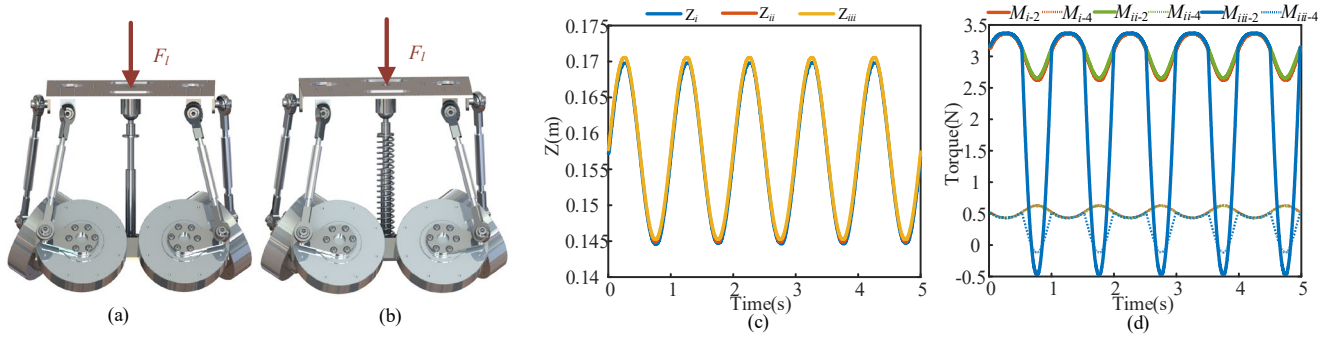

Fig. 9. (a) and (b) are schematic diagrams of the torso under axial load, (a) without spring and (b) with spring. (c) and (d) are data curves during experiments, (c) for position *Z*, (d) joint torque. (*i*) position control without spring, (*ii*) and (*iii*) are force-position hybrid controls, but (*ii*) without spring and (*iii*) with spring, where 2 and 4 are motor numbers.

spring, and (*iii*) force-position hybrid control with spring (Fig. 9. (b)). The trajectory of the moving platform for each experiment is $Z = 0.158 + 0.013(2\pi t)$, and the duration is 5s. Changes in position *Z* of the torso (Fig. 9. (c)) did not differ much among the three experiments. As the torque changes for each motor are identical during the motion of the torso, torque values for motors 2 and 4 are presented in Fig. 9. (d). The results indicate little difference in motor torque between experiments (*i*) and (*ii*). However, the inclusion of the compression spring significantly reduces the motor torque. It can be observed that the passive spring assists in absorbing the pressure from external loads, reducing the motors' energy consumption.

B. *Stretching Experiment*

The static position of the bionic torso is defined as Z=0.158m, φ=0°, θ=0°, ψ=0°. After the robot stood stably for 5 s, the bionic torso was extended for ten cycles following the trajectory $Z = 0.158 + 0.015 \times \sin(2\pi t)$. The position and joint torques of the torso during the experiment are depicted in Figs. 10(d) and (e). As can be observed from the experimental video, each cycle of torso motion extends and pushes the robot's hind limbs backward, then contracts to pull the rear body forward. From the torque of each limb of the robot (as shown in Figs. 10. (h) and (i)), it can be observed that each limb can coordinate with the extending torso. The experimental results demonstrate that the active torso enables the quadruped robot to possess the ability to extend and contract. The torso proposed in this study is well-suited for application in quadruped robots.

C. *Lateral Bending Experiment*

We selected one of the three rotational movements of the bionic torso for experimentation - laterally bending. In this

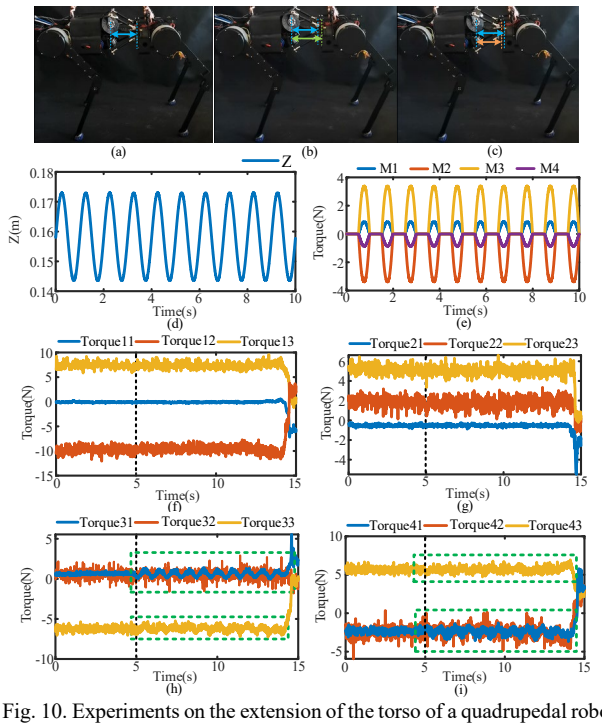

Fig. 10. Experiments on the extension of the torso of a quadrupedal robot during standing. Snapshots (a), (b), and (c) depict the robot during torso extension motion, while (d) shows position *Z* of the torso, and (e) illustrates the torso torque *M*. Additionally, (f), (g), (h), and (i) represent the joint motor torques of the robot's legs, where (f) corresponds to the right front leg, (g) to the right rear leg, (h) to the left rear leg, and (i) to the left front leg.

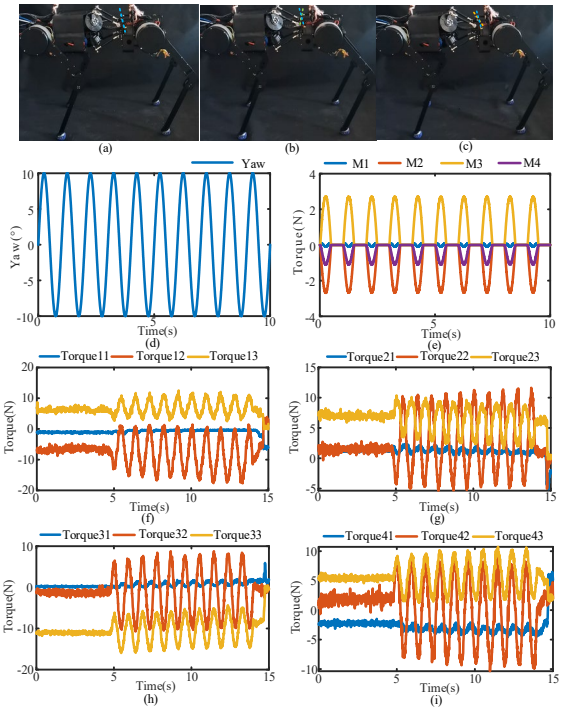

Fig. 11. Experiments on lateral bending of the torso of a quadrupedal robot during standing. Snapshots (a), (b), and (c) depict the robot during lateral bending motion of the torso, while (d) shows yaw angle of the torso, and (e) illustrates the torso torque *M*. Additionally, (f), (g), (h), and (i) represent the joint motor torques of the robot's legs, where (f) corresponds to the right front leg, (g) to the right rear leg, (h) to the left rear leg, and (i) to the left front leg.

experiment, the torso bent laterally (Fig. 11. (d)) for ten cycles following the trajectory $\varphi = 10(2\pi t)$ after the robot had stood stably for 5s. Moreover, the joint torques (Fig. 11. (e)) of the torso vary regularly. During torso motion, the moving platform induces lateral swinging of the robot's rear body around the axis of the robot. The limbs of the quadruped robot exhibit good coordination with the torso, as evident from the torque of each joint in the quadruped robot's limbs (Fig. 11. (f), (g), (h), (i)). Similarly, the bionic torso enables the quadruped robot's body to achieve sagittal bending and axial twisting. Thus, it can be concluded that the proposed torso enhances the flexibility of the quadruped robot, allowing the robotic body to mimic various flexible movements of quadruped animals.

VI. Conclusion

This paper presents an active bionic torso for quadruped robots, which emulates animal torsos' morphological features and functional movements. It possesses an excellent range of flexion and extension, as well as lateral bending range, compared to cats and horses. Additionally, it can withstand axial loads that are ten times the robot's weight. The torso responds well to a wide frequency range and has a substantial range of motion dexterity. The bionic torso is capable of accurately executing movement commands under active control. The passive springs within the torso, mimicking the intervertebral discs, can passively cushion the load. Ultimately, the active bionic torso mounted on a quadruped robot can exhibit animal torso movements, enhancing the robot's mobility and stability. In subsequent research, we will apply bionic control theory [19] [25] [26] [27] to the quadruped robot featuring a bionic active torso designed in this research, and explored the coordination mechanism between the torso and limbs during movement.

References

[1] J. W. Hermanson, A. De Lahunta, *Miller and Evans' anatomy of the dog-E-book*. Amsterdam: Elsevier Health Sciences. 2018, ch. 4-7.

[2] R. Kawasaki, R. Sato, E. Kazama, A. Ming, and M. Shimojo, "Development of a flexible coupled spine mechanism for a small quadruped robot," in *2016 IEEE International Conference on Robotics and Biomimetics*, 2016, pp. 71-76.

[3] C. L. Wang, C. Fan, Y. Yang, M. Zhan, H. Shao, and B. Ma, "Realization of a bio-inspired cheetah robot with a flexible Spine," in *2020 IEEE International Conference on Mechatronics and Automation*, 2020, pp. 1185-1190.

[4] G. Chen, M. Ma, S. Guo, H. Lu and B. Cai, "Mechanism design and performance analysis of bionic quadruped robot with spine," in *40th Chinese Control Conference*, Shanghai, China, 2021, pp. 6685-6690.

[5] S. Seok, A. Wang, M. Y. Chuah, D. J. Hyun, J. Lee, D. Otten, J. Lang and S. Kim, "Design principles for energy-efficient legged locomotion and implementation on the MIT cheetah robot," *IEEE/ASME Transactions on Mechatronics*, vol. 20, no. 3, pp. 1117-1129, 2015.

[6] P. Eckert, A. Spröwitz, H. Witte and A. J. Ijspeert, "Comparing the effect of different spine and leg designs for a small bounding quadruped robot," in 2015 *IEEE International Conference on Robotics and Automation*, 2015, pp. 3128-3133.

[7] Q. Shi, J. Wang, S. Quan, X. Jia, Q. Huang and T. Fukuda, "Development of a small-sized quadruped robotic rat capable of multimodal motions," *IEEE Transactions on Robotics*, vol. 38, no. 5, pp. 3027-3043, 2022.

[8] Z. Li and Y. G. Tan, "Trotting motion of the quadruped model with two spinal joints and its dynamics features," *Journal of Robotics*, vol. 2020, no. 1, 2020.

[9] S. Bhattacharya, A. Singla, D. Dholakiya, S. Bhatnager, B. Amrutur, A. Ghosal and S. Kolathaya, "Learning active spine behaviors for dynamic and efficient locomotion in quadruped robots," in *28th IEEE International Conference on Robot and Human Interactive Communication*, 2019, pp. 1-6.

[10] K. Ye and K. Karydis, "Modeling and trajectory optimization for standing long jumping of a quadruped with a preloaded elastic prismatic spine," in *IEEE/RSJ International Conference on Intelligent Robots and Systems*, 2021, pp. 902-908.

[11] L. Li, S. Ma, I. Tokuda, F. Asano, M. Nokata, Y. Tian, and L. Du, "Synergetic effect between limbs and spine dynamics in quadruped walking robots," in *IEEE International Conference on Robotics and Automation*, 2021, pp. 6818-6823.

[12] S. Suzuki, T. Kano, A. J Ijspeert, and A. Ishiguro, "Sprawling quadruped robot driven by decentralized control with cross-coupled sensory feedback between legs and torso," *Frontiers in Neurorobotics*, vol. 14, pp. 607455, 2021.

[13] B. Chong, Y. O. Aydin, C. Gong, G. Sartoretti, Y. Wu, J. Rieser, H. Xing, J. Rankin, K. Michel, A. Nicieza, J. Hutchinson, D. Goldman and H. Choset, "Coordination of back bending and leg movements for quadrupedal locomotion," in *14th* Conference on *Robotics*: *Science and Systems*, 2018.

[14] P. Arnold, "Evolution of the mammalian neck from developmental, morpho-functional, and paleontological perspectives," *Journal of Mammalian Evolution*, vol. 28, no. 2, pp. 173-183, 2021.

[15] Q. Zhao, H. Sumioka, K. Nakajima, X. X. Yu, and R. Pfeifer, "Spine as an engine: effect of spine morphology on spine-driven quadruped locomotion," *Advanced Robotics*, vol. 28, no. 6, pp. 367-378, 2014.

[16] F. Galbusera, T. Bassani, "The spine: a strong, stable, and flexible structure with biomimetics potential," *Biomimetics*, vol. 4, no. 3, pp. 60, 2019.

[17] D. W. Hukins, "Disc structure and function," in *Biology Of Invertebral Disc*. Boca Raton: CRC Press, 2019, pp. 1-38.

[18] M. Mirzaeipoueinak, H. S. Mordechai, S. S. Bangar, M. Sharabi, J. L. Tipper, and J. Tavakoli, "Structure-function characterization of the transition zone in the intervertebral disc," *Acta Biomaterialia*, vol. 160, pp. 164-175, 2023.

[19] Y. G. Zhu, S. J. Zhou, M. Poramate, and R. Y. Li, "Design, analysis, and neural control of a bionic parallel mechanism," *Frontiers of Mechanical Engineering*, vol. 16, no. 3, pp. 1-19, 2021.

[20] J. M. Macpherson and Y. Ye, "The cat vertebral column: stance configuration and range of motion," *Experimental Brain Research*, vol. 119, no. 3, pp.324-332, 1998.

[21] M. Faber, C. Johnston, H. C. Schamhardt, P. R. Van Weeren, L. Roepstorff, and A. Barneveld, "Three-dimensional kinematics of the equine spine during canter," *Equine Veterinary Journal*, vol. 33, no. S33, pp. 145-149, 2001.

[22] T. H. Smit, "The use of a quadruped as an in vivo model for the study of the spine–biomechanical considerations," *European Spine Journal*, vol. 11, no. 2, pp. 137-144, 2002.

[23] P. Ataei, Z. Anvari and M. T. Masouleh, "Kinetostatic performance and collision-free workspace analysis of a 3-DOF delta parallel robot," in *5th RSI International Conference on Robotics and Mechatronics*, 2017, pp. 576-581.

[24] Y. G. Zhu, M. H. Zhang, X.Y. Zhang, H. P. Qin, "Dynamic compliance and energy-saving legged elastic parallel joints for quadruped robots: design and realization," *Frontiers of Mechanical Engineering*, vol. 19, no. 2, pp. 13, 2024.

[25] Y. G. Zhu, R. Y. Li, and Z. P. Song, "Bionic muscle control with adaptive stiffness for bionic parallel mechanism," *Journal of Bionic Engineering*, vol. 20, no. 2, pp. 598-611, 2023.

[26] Y. G. Zhu, S. J. Zhou, D. X. Gao, "Synchronization of non-linear oscillators for neurobiologically inspired control on a bionic parallel waist of legged robot," *Frontiers in Neurorobotics*., vol. 13, pp. 59-60, 2019.

[27] Y. G. Zhu, L. Zhang, P. Manoonpong, "Generic mechanism for waveform regulation and synchronization of oscillators: An application for robot behavior diversity generation," *IEEE Transactions on Cybernetics*, vol. 52, no. 6, pp. 4495-4507, 2022.